COMMUNICATION

Three-Dimensional Carrier Profiling of Individual Si Nanowires by Scanning Spreading Resistance Microscopy

By *Xin Ou,* Pratyush Das Kanungo,* Reinhard Kögler, Peter Werner, Ulrich Gösele, Wolfgang Skorupa,* and *Xi Wang*

Individual silicon nanowires (Si NWs) grown by molecular beam epitaxy and in situ doped with boron were investigated by scanning spreading resistance microscopy (SSRM), a technique based on conductive atomic force microscopy. The carrier profiles of the NWs were derived from the measured spreading resistance values and calibrated with the known carrier concentration of the underlying epilayer. The 3D-SSRM profile of a NW was obtained by measuring the NW cross sections at different depths along the radial direction. Scanning the same NW with a controlled force on the SSRM tip can abrade material from the cross-sectional surface and the tip moves deeper into the volume of the NW after each image is scanned. Repeated stripping of the material from the NW results in a "thinning" of the remaining NW segment and a corresponding increase of its resistance, which can be addressed by an appropriate data correction. The achieved three-dimensional carrier profile reveals a multishell structure of the carrier distribution across the NW diameter, which consists of a lower doped core region, a higher doped shell region, and a carrier depleted subsurface region.

Si nanowires are considered promising candidates for incorporation into the next generation of electronic devices.[1,2] Vertical Si NWs on Si substrate are commonly grown based on the so-called vapor–liquid–solid (VLS)[3,4] method by different techniques such as chemical vapor deposition (CVD)[5] and molecular beam epitaxy (MBE).[6] Doping of Si NWs has already been demonstrated using in situ[5,7–9] and ex situ[10,11] techniques. In order to precisely control the doping process for device fabrication it is imperative to understand the electrical properties of the doped Si NWs, especially the spatial distribution of the dopants in the NWs. Due to their large surface-to-volume ratio, a strong surface segregation of dopants in NWs was theoretically predicted by ab intio calculation[12,13]

and experimentally investigated by atom probe tomography,[14] Raman scattering,[15,16] scanning photocurrent microscopy,[17] electron holography,[18] and electrical transport measurements in connection with surface etching.[19] Moreover, the dopant deactivation at the NW surface was demonstrated by measuring the electrical conduction of doped NWs with different diameters.[20,21] However, detailed analysis of these effects in combination requires a volumetric mapping of the dopant distribution on various cross sections of an individual NW. Very recently it was shown that SSRM can be applied to obtain the two-dimensional carrier profile across the cross section of a doped Si NW.[22,23] In this paper the capability of three-dimensional carrier profiling of individual Si NWs by SSRM is demonstrated.

SSRM is an established analytical technique for two-dimensional carrier profiling in semiconductor materials and devices.[24,25] The electrical circuit for the SSRM measurement consists of an SSRM probe tip, the sample, and a logarithmic current amplifier for the data readout. A constant bias is applied between the tip and the sample. The current passes through a serial resistor which includes the tip resistance (R_{tip}), the contact resistance (R_c) between the tip and the sample, the spreading resistance (R_S), and the resistance of the investigated material which consists of the Si substrate (R_{bulk}) and the connected NW (R_{NW}). The resistance measured is the sum of the above components and is given by:

$$R = R_S + R_{tip} + R_c + R_{bulk} + R_{NW} \qquad (1)$$

Among the component resistances only R_S gives a local measure of the electrical characteristics of the sample and can be estimated by the formula[26]

$$R_S = \rho / 4a \qquad (2)$$

for an ideal Ohmic contact between a cylindrical tip and the sample surface, where ρ is the local sample resistivity and a is the radius of the effective contact which defines the spatial resolution of the measurement. The state-of-the-art resolution amounts to about 10 nm or even below.[24,25] In order to keep R_S as the dominant resistance ($R_S \approx R$) a large tip force in the range of 1–100 µN is applied to achieve a preferentially low R_c. Moreover, a diamond-coated conductive Si tip is used to obtain a low R_{tip} and a high wear resistance for high durability of the tip during the forceful scanning. The characteristics of a hard conductive tip and the application of a high tip force in SSRM provide the ability for three-dimensional carrier profiling of Si NWs. The capability of

[*] Dr. X. Ou, P. D. Kanungo, Dr. P. Werner, Prof. U. Gösele
Max Planck Institute of Microstructure Physics
Weinberg 2, Halle D-06120 (Germany)
E-mail: X.ou@fzd.de; kanungo@mpi-halle.de
Dr. X. Ou, Dr. R. Kögler, Dr. W. Skorupa
Institute of Ion Beam Physics and Materials Research
Forschungszentrum Dresden–Rossendorf e.V.
P.O. Box 510119, 01314 Dresden (Germany)
Dr. X. Ou, Prof. X. Wang
Shanghai Institute of Microsystem and Information Technology
Chinese Academy of Sciences
Shanghai 20050 (P.R. China)

a 3D-SSRM profiling on InP was already reported by Eyben et al.[27]

NWs with 50 to 250 nm diameters and lengths between 100 and 400 nm were grown by MBE under ultrahigh vacuum conditions (10^{-10} mbar) on (111) Si using Au as growth initiator at a temperature of 525 °C. The NWs were in situ doped with boron during the growth. The resistivity of the substrate was 10 Ω cm corresponding to a carrier concentration of 1.3×10^{15} cm^{-3} and the expected boron concentration of the doped NWs, as well as the epilayer[6] that grows with it, was 10^{19} cm^{-3}. Experimental details were reported elsewhere.[7]

The cross-sectional NW specimens for SSRM measurements were fabricated as follows. First, a layer of about 400 nm SiO$_2$ was deposited on the sample by magnetron sputtering to cover the NWs. Second, the specimens were cut and glued against each other using the preparation procedures usually applied for cross-sectional transmission electron microscopy. Afterwards, the cross-sectional surface was polished with SiC powder and diamond powder. The cross-sectional specimens were investigated by scanning electron microscopy (SEM) to detect the positions of the NWs. SSRM measurements were subsequently performed using a multi-mode AFM instrument (from Veeco Instruments, Camarillo, CA) with an SSRM module. A constant bias voltage of −2.5 V was applied between the tip and the sample during scanning. A deflection voltage between 0.2 and 1 V was used to generate a force so that the tip definitely indents the sample surface and moves deeper into the volume. During the measurements, the tip was scanned perpendicular to the Si/SiO$_2$ interface in the axial direction of the NW.

Figure 1 shows an image of the spreading resistance where the Si substrate (Sub), the epilayer (Epi), and the SiO$_2$ layer are indicated. The cross section of this specific NW is 237 nm wide and 368 nm long. The dark area surrounding the NW indicates the insulating characteristic of SiO$_2$ with a high resistance (HR). The brighter color of the NW and of the epilayer indicates a lower resistance as compared to the Si substrate. Darker stripes of higher resistance in the substrate and epilayer can be ascribed to scratches formed during polishing. The fine dotted lines (parallel to the NW axis), visible in the NW and in the epilayer below, are tip traces caused by the SSRM prescan. The respective profile of R_S in the axial direction of the NW is shown on the right side. R_S is converted to carrier concentrations by scaling with the known resistivity of the epilayer of 8.58×10^{-3} Ω cm, corresponding to a carrier concentration of 10^{19} cm^{-3}. The calibration is based on the linear relation between R_S and ρ according to Equation (2), and the carrier concentrations can be extracted from the ρ data using the standard curve of the carrier concentration versus resistivity for silicon.[28] The resistivity fluctuations of the substrate and epilayer range observed in the axial profile (Figure 1) are mainly due to the surface defects (scratches) left from the polishing of the sample. These scratches introduce high-resistance lines which are mostly parallel to the radial direction of the NW. However, this effect has not been found in the region of the investigated NW. Measuring the resistivity profile from a uniformly doped and flat Si substrate, relatively small variations, below 10%, of the R_S values are obtained. Scanning is repeated over the same
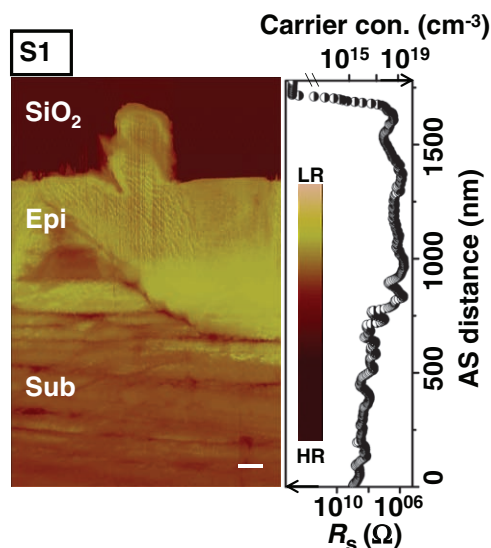
Figure 1. Cross-sectional SSRM image of an individual Si NW standing on the epitaxial Si layer (Epi) and the Si substrate (Sub). The NW is embedded in a SiO$_2$ layer. Dark and bright colors indicate high (HR) and low (LR) resistance, indicated by the scale bar on the right side. S1 denotes the first scan of this NW. The spreading resistance (R_S) profile in axial scanning direction (AS) averaged over the whole NW range is shown by the curve on the right side. The carrier concentration (vertical axis) is converted from R_S, and calibrated from the known resistivity of the epilayer using the standard carrier concentration vs resistivity curve (Ref. [26]). The bar inserted in the left image denotes a length of 100 nm.

NW in order to investigate one individual NW in three dimensions by SSRM. During scanning, the scratching of the tip over the NW cross-sectional surface abrades some material, and the tip moves deeper into the volume with successive image scans. The sequence of the NW cross sections (S2 → S5) for consecutive scans of the same NW shown in Figure 1 (S1) is shown in **Figure 2a**. Obviously, the radial width of the SSRM profile shrinks gradually and the top part of the NW vanishes after scanning five times. After the sixth scan the NW completely disappeared. Figure 2b shows the typical morphology of a vertical column-shaped Si NW after removing the Au droplet from the top by wet etching. The shrinking of the NW cross-section in Figure 2a can easily be understood considering that the investigated NW cross section shifts with every image scan toward a deeper position as schematically illustrated in Figure 2c. Assuming that the NW segment in S1 (Figure 1) is a half column of width $2r$ and of thickness $d = r$, the radial cross-section area is $A = \frac{1}{2}\pi r^2$. Material stripping from the surface of this specimen results in the shrinking of the thickness (d) as well as the radial cross section area (A) of the remaining NW segment. The change of d and A by repeated scanning from S1 to S5 is calculated from the width of the cross sections (see Supporting Information).

The carrier profiles of the NW cross-sections (see Figure 2a) can be derived from R_S using the same method demonstrated in Figure 1. However, as A decreases (from S1 to S5) the measured spreading resistance R_S can be overestimated due to

(a)

(b)

(c)
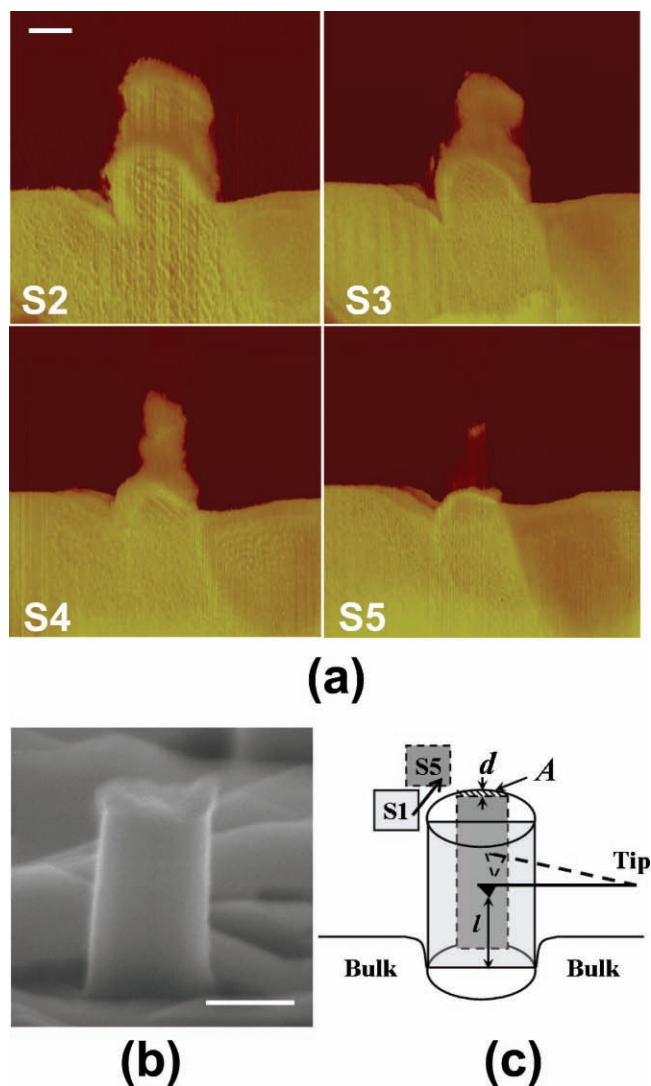
Figure 2. a) SSRM images showing a sequence of cross sections of the same NW as shown in Figure 1 obtained by repeated scanning of this NW. S2 means the second scan and S5 the fifth scan. Dark and bright colors indicate high and low resistance. b) SEM image of a typical free-standing vertical Si NW after removing the Au cap on the top. c) Schematic of the shift of the measuring Si NW cross section area due to scanning from S1 to S5. A and d denote the radial cross-section area (dashed area of S5) and the thickness of the remaining segment of the NW. l is the distance between the actual tip position and the bottom of the NW. The bars inserted in (a) and (b) denote a length of 100 nm.

the remarkable increase in the resistance of the remaining NW segment,

$$R_{NW} = \rho l / A \tag{3}$$

R_{NW} (in Equation (1)) increases, whereas $R_{bulk} = R_{Sub} + R_{Epi}$ is negligible due to the very large cross-sectional area of the substrate (R_{Sub}) and the epilayer (R_{Epi}) compared to the NW.

Assuming ρ remains constant for a single image scan, the increase of R_{NW} (due to the decrease of A and the increase of l)

can be quantitatively estimated by combining Equation (2) and (3) as follows:

$$R_{NW}/R_S = \frac{\rho l / A}{\rho / 4a} \approx 4al / A = k \tag{4}$$

For the same imaged cross section k only depends on the distance (l, see Figure 2c) between the actual tip position and the bottom of the NW ($l = 0$). Therefore, the resistivity values measured close to the top of the NW cross sections are not directly comparable to those measured at the bottom. Nevertheless, the R_S profiles extracted from the NW cross-sections (S1 through S5) can be corrected by $R_S = R/(k + 1)$, where $R \approx R_S + R_{NW}$ is the measured resistance value. However, in the case of S1 (Figure 1) the body of the NW cross section is thick enough and k is too small to result in a significant change of the resistivity values measured along the NW.

Figure 3 presents profiles of R_S along the radial NW direction (RS) as derived from the NW cross sections shown in Figure 1 and Figure 2a. These profiles are extracted from the length position at $l = 0.75\ l_{NW}$, where l_{NW} means the total length of the NW and the resistivity values are corrected by eliminating the influence of R_{NW} as described above. R_S values are taken from a 512 × 512 data matrix along the radial direction at a distance of 1.9 nm. The carrier concentration of the curves is scaled on the right axis. According to the RS profile of S1 the carrier
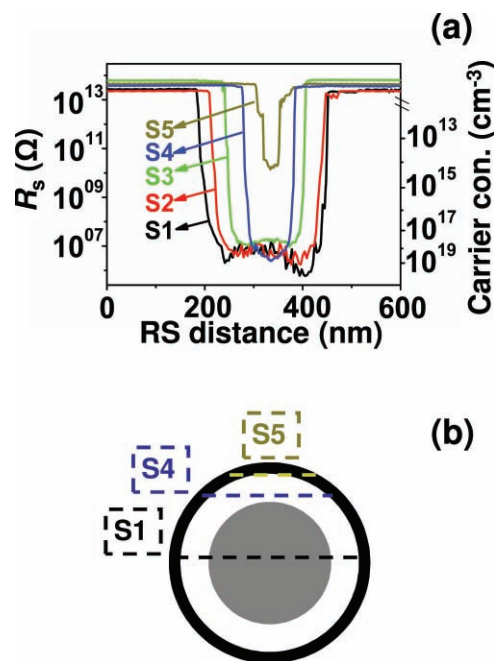
Figure 3. a) Spreading resistance (R_S) profiles taken from NW cross sections S1 (Figure 1) to S5 (Figure 2a) are shown in radial scanning direction (RS). The profiles are corrected by elimination of the influence of R_{NW} on the measurement of R_S. The carrier concentration (right axis) is converted and calibrated using the same method described for Figure 1. b) Scheme of a multishell structure of the carrier distribution across the NW diameter consisting of the core region (gray), the higher doped shell region (white ring), and the carrier-depleted surface (outer black ring). The relative positions of the cross sections S1, S4, and S5 are indicated by the dashed lines.

concentration close to the surface of the NW peaks at 10^{19} cm^{-3}. This is the same level as in the epilayer and one order of magnitude higher than in the core region. The same difference in the carrier concentrations between core and shell of the NW also appears in the RS profiles taken from other length positions of the S1 cross section. The difference in the carrier concentration measured in the core and shell is significantly beyond the fluctuation induced by the error of the SSRM measurement, which is estimated to be below 10%. The thickness of the highly doped shell region is around 30 nm. Except for S5, the carrier concentration of the sequential NW cross sections is of the same order of magnitude. Interestingly, the radial profiles S2 and S3 confirm the core-shell structure demonstrated in profile S1 and exhibit a similar concave shape, whereas S4 and S5 change to a convex profile shape. The thickness of the NW segment in S4 and S5 is reduced to less than 10% of the original one in S1 (see Supporting Information). For that reason the NW segment S4, with a calculated thickness of 12 nm, is fully incorporated in the highly doped outer-shell region of 30 nm thickness surrounding the core of the NW. This is schematically demonstrated by Figure 3b. The higher number of electrically active dopants in the shell may result from inhomogeneous doping during in situ dopant incorporation into the NW. For CVD-grown, doped Si NWs it was suggested that this core-shell structure mainly arises from the additional dopant deposition at the NW surface by a vapor-solid (VS) mechanism.[14] However, it is worth noting that the NW investigated here was grown and in situ boron doped under ultrahigh vacuum by MBE. Theoretical papers based on NWs of a few nanometer diameter speculated about the surface segregation of boron due to less energetic positions at the surface.[12,13] In our study the NW diameter is significantly larger than a few nanometres. Surface segregation of boron was also observed in MBE-grown planar epitaxial Si films.[29,30] Another possible effect for p-type doping in the shell region is the incorporation of Au remaining from the growth-initiating phase.[31] However, this should be negligible as the solubility of Au in Si is less than 10^{15} cm^{-3} at the growth temperature.[32] A detailed investigation of the distribution of the total dopant concentration (both electrically active and deactivated) by techniques such as atom probe tomography is required to make conclusions about the exact origin of this core-shell structure.

Generally, the unpassivated NW is covered by the native SiO$_2$ surface layer (1–2 nm), and the electrical properties of the NW are assumed to be influenced by the quality of the Si/SiO$_2$ interface.[20,33] The interface states act as carrier traps (both for electrons and for holes) causing a depleted region of a certain thickness close to the NW surface. The remaining NW segment in S5 with a calculated thickness $d = 2.6$ nm is almost entirely located inside the depleted surface region (Figure 3b) which is estimated to be $d_D = 2.5$ nm according to the model given by Seo et al.:[20]

$$d_D = r_{phys} \left(1 - \sqrt{1 - \frac{2}{r_{phys}} \frac{N_S}{N_A}} \right) \qquad (5)$$

where r_{phys} is the physical radius of 167 nm (Figure 1), and N_S and N_A are the surface charge density (2×10^{12} cm^{-2})[20] and the dopant concentration (10^{19} cm^{-3}). This may result in a lower

carrier concentration, as shown in the curve S5 of Figure 3a. Moreover, it was suggested that the dielectric mismatch between the Si NW ($\varepsilon_{Si} = 11.7$) and its surrounding ($\varepsilon_{SiO2} = 3.9$ or $\varepsilon_{air} = 1$) also increases the ionization energy and therefore reduces the activation of the dopants.[2,21,34] Considering its radius-dependent character this effect especially decreases the activation degree of dopants located very close to the NW surface.

Both the removal and the uncovering of NWs after several SSRM image scans are confirmed by the SEM image in **Figure 4**. These two SEM images show the same specimen area mapped before and after the SSRM investigation. By comparison, the lower NW visible in Figure 4a is completely removed after several scans (Figure 4b). On the contrary, the upper NW is fully revealed and significantly more pronounced after several SSRM image scans. The NW material is abraded by SSRM in a controlled manner. The uncovering of an NW partly buried in the oxide layer by the SSRM imaging scans is demonstrated in the supporting materials. It is worth noting that the probe tip indents the sample surface during the measurement and measures the characteristics of the material below the surface. The depth of this indentation is controlled by adjusting the deflection bias (0.2 to 1 V) which generates a corresponding tip force. The influence of surface defects can be minimized by enhancing the tip force, however, this may compromise the spatial resolution of the measurement.[35] Optimum conditions are achieved using an appropriate tip force. By moving the tip forward, the specimen surface is destroyed and can be pushed away as is visible in Figure 4b.

In conclusion, the capability of the SSRM measurement for the three-dimensional profiling of electrical carriers in individual NWs is demonstrated via a stepwise shift of the measured NW cross section toward deeper positions in the specimen
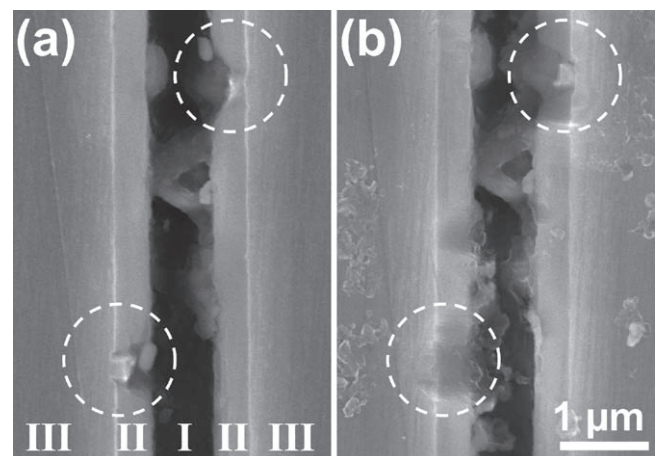
Figure 4. SEM images of the same specimen area before a) and after b) the SSRM measurement. Two samples, each with one NW, are glued together face-to-face. The positions of the NW locations are indicated by dashed circles. Layers denoted by I, II, and III are glue, the SiO$_2$ layer, and the Si substrate, respectively. Bright spots located close to the Si NWs in (a) are grains remaining from polishing powder, as confirmed by energy dispersive spectroscopy (EDX). Some material that was moved away by the SSRM tip is visible in (b) along the right and left sides.

by abrading material during repeated SSRM scanning. The measured spreading resistance is corrected by eliminating the influence of the resistance of the remaining NW body, acting as a parasitic resistance. The carrier profiles of the NWs are determined from the measured spreading resistance and calibrated by the known carrier concentration of the underlying epilayer. A model is provided considering the increase in R_{NW} with increasing length and decreasing diameter of the NW segment. It is found that the carrier distribution across the NW diameter is characterized by a multishell structure of "lower doped core–higher doped shell–depleted surface". The influence of the Si/SiO_2 interface (carrier depletion) on the carrier concentration is demonstrated by measuring the cross section of a very thin NW segment (S5).

Supporting Information

Supporting Information is available from the Wiley Online Library or from the author. The Supporting Information shows the decrease of the calculated radial cross-sectional area A and the thickness d of the NW segments (S1 to S5) which are shown in Figure 1 and Figure 2a. Moreover, an NW partially buried under oxide is uncovered, as demonstrated by SSRM imaging scans.

Acknowledgements

[1] C. Thelander, P. Agarwal, S. Brongersma, J. Eymery, L. F. Feiner, A. Forchel, M. Scheffler, W. Riess, B. J. Ohlsson, U. Gösele, L. Samuelson, *Mater. Today* **2006**, *9*, 28.

[2] V. Schmidt, J. V. Wittemann, S. Senz, U. Gösele, *Adv. Mater.* **2009**, *21*, 2681.

[3] R. S. Wagner, W. C. Ellis, *Appl. Phys. Lett.* **1964**, *4*, 89.

[4] E. I. J. Givargizov, *J. Cryst. Growth* **1975**, *31*, 20.

[5] Y. Cui, X. Duan, J. Hu, C. M. Lieber, *J. Phys. Chem. B* **2000**, *104*, 5213.

[6] P. Werner, N. D. Zakharov, G. Gerth, L. Schubert, U. Gösele, *Int. J. Mater. Res.* **2006**, *97*, 1008.

[7] P. D. Kanungo, N. Zakharov, J. Bauer, O. Breitenstein, P. Werner, U. Gösele, *Appl. Phys. Lett.* **2008**, *92*, 263107.

[8] K. K. Lew, L. Pan, T. E. Bogart, S. M. Dilts, E. C. Dickey, J. M. Redwing, Y. F. Wang, M. Cabassi, T. S. Mayer, S. W. Novak, *Appl. Phys. Lett.* **2004**, *85*, 3101.

[9] G. Zheng, W. Lu, S. Jin, C. M. Lieber, *Adv. Mater.* **2004**, *16*, 1890.

[10] S. Hoffmann, J. Bauer, C. Ronning, Th. Stelzner, J. Michler, C. Ballif, V. Sivakov, S. H. Christiansen, *Nano Lett.* **2009**, *9*, 1341.

[11] P. D. Kanungo, R. Kögler, K. Nguyen-Duc, N. Zakharov, P. Werner, U. Gösele, *Nanotechnology* **2009**, *20*, 165706.

[12] M. V. Fernandez-Serra, C. Adessi, X. Blase, *Phys. Rev. Lett.* **2006**, *96*, 166805.

[13] H. Peelaers, B. Partoens, F. M. Peeters, *Nano Lett.* **2006**, *6*, 2781.

[14] D. E. Perea, R. E. Hemesath, E. J. Schwalbach, J. L. Lensch-Falk, P. W. Voorhees, L. J. Lauhon, *Nat. Nanotechnol.* **2009**, *4*, 315.

[15] G. Imamura, T. Kawashima, M. Fujii, C. Nishimura, T. Saitoh, S. Hayashi, *Nano Lett.* **2008**, *8*, 2620.

[16] N. Fukata, *Adv. Mater.* **2009**, *21*, 2829.

[17] J. E. Allen, D. E. Perea, R. E. Hemesath, L. J. Lauhon, *Adv. Mater.* **2009**, *21*, 3067.

[18] M. I. Den Hertog, H. Schmid, D. Cooper, J. L. Rouviere, T. M. Björk, H. Riel, P. Rivallin, S. Karg, W. Riess, *Nano Lett.* **2009**, *9*, 3837.

[19] P. Xie, Y. J. Hu, Y. Fang, J. J. Huang, C. M. Lieber, *Proc. Nati. Acad. Sci. USA* **2009**, *106*, 15254.

[20] K. Seo, S. Sharma, A. A. Yasseri, D. R. Stewart, T. I. Kamins, *Electochem. Solid St. Lett.* **2006**, *9*, G69.

[21] M. T. Bjoerk, H. Schmid, J. Knoch, S. Riel, W. Riess, *Nat. Nanotechnol.* **2009**, *4*, 103.

[22] X. Ou, P. Das Kanungo, R. Kögler, P. Werner, U. Gösele, W. Skorupa, X. Wang, *Nano Lett.* **2009**, *10*, 171.

[23] T. Hantschel, C. Demeulemeester, P. Eyben, V. Schulz, O. Richard, H. Bender, W. Vandervorst, *Phys. Status Solidi A* **2009**, *206*, 2077.

[24] K. Maknys, O. Douherets, S. Anand, *Appl. Phys. Lett.* **2003**, *83*, 2184.

[25] D. Alvarez, J. Hartwich, M. Fouchier, P. Eyben, W. Vandervorst, *Appl. Phys. Lett.* **2003**, *82*, 1724.

[26] D. K. Schroder, *Semiconductor Material and Device Characterization, 3rd Edition*, John Wiley & Sons, New Jersey **2006**, p. 31.

[27] P. Eyben, W. Vandervorst, D. Alvarez, M. Xu, M. Fouchier, in *Scanning probe microscopy*, (Eds: S. Kalinin and A. Gruverman), Springer, New York, **2007**, Chapter I.2. p.82.

[28] R. F. Pierret, *Advanced Semiconductor Fundamentals*, 2nd ed., Prentice Hall, Upper Saddle River, NJ, **2003**.

[29] Y. Kumagai, K. Ishimoto, R. Mori, F. Hasegawa, *J. Cryst. Growth* **1995**, *150*, 989.

[30] T. Tatsumi, H. Hirayama, N. Aizaki, *Jpn. J. Appl. Phys.* **1988**, *27*, L954.

[31] M. C. Putnam, M. A Filler, B. M. Kayes, M. D. Kelzenberg, Y. Guan, N. S. Lewis, J. M. Eiler, H. A. Atwater, *Nano Lett.* **2008**, *8*, 3109.

[32] F. A. Trumbore, *Bell Syst. Tech. J.* **1960**, *39*, 205.

[33] V. Schmidt, S. Senz, U. Gösele, *Appl. Phys. A – Mater. Sci. Process.* **2007**, *86*, 187.

[34] M. Diarra, Y.-M. Niquet, C. Delerue, G. Allan, *Phys. Rev. B* **2007**, *75*, 045301.

[35] A. Suchodolskis, A. Hallén, J. Gran, T.-E. Hansen, U. O. Karlsson, *Nucl. Instrum. Methods B* **2006**, *253*, 141.